Zernike wavefront sensor modeling development for LOWFS on WFIRST-AFTA

Xu Wang, J. Kent Wallace, Fang Shi
Jet Propulsion Laboratory, California Institute of Technology, Pasadena, CA 91109-8099

ABSTRACT

WFIRST-AFTA design makes use of an existing 2.4m telescope for direct imaging of exoplanets. To maintain the high contrast needed for the coronagraph, wavefront error (WFE) of the optical system needs to be continuously sensed and controlled. Low Order Wavefront Sensing (LOWFS) uses the rejected starlight from an immediate focal plane to sense wavefront changes (mostly thermally induced low order WFE) by combining the LOWFS mask (a phase plate located at the small center region with reflective layer) with the starlight rejection masks, i.e. Hybrid Lyot Coronagraph (HLC)'s occulter or Shaped Pupil Coronagraph (SPC)'s field stop. Zernike wavefront sensor (ZWFS) measures phase via the phase-contrast method and is known to be photon noise optimal for measuring low order aberrations. Recently, ZWFS was selected as the baseline LOWFS technology on WFIST/AFTA for its good sensitivity, accuracy, and its easy integration with the starlight rejection mask. In this paper, we review the theory of ZWFS operation, describe the ZWFS algorithm development, and summarize various numerical sensitivity studies on the sensor performance. In the end, the predicted sensor performance on SPC and HLC configurations are presented.

Key words: Wavefront sensing, Zernike phase contrast, WFIRST-AFTA, LOWFS

1. INTRODUCTION

Wide-Field InfraRed Survey Telescope (WFIRST) was the top-ranked large space mission in the New Worlds New Horizons Decadal Survey of Astronomy and Astrophysics in 2010. When the two existing 2.4 meter diameter telescopes known as the Astrophysics Focused Telescope Assets (AFTA) were made available to NASA, one of them was selected for WFIRST-AFTA mission concept. Later in 2013, a coronagraph instrument (CGI) was added to the payload as the second instrument. The WFIRST-AFTA Coronagraph will be the first high contrast stellar coronagraph in space intended for imaging, discovery, and spectral characterization of exoplanets.

WFIRST observatory demands in the order of tens of pm optical wavefront stability to achieve the required level of starlight suppression with ~1e-9 coronagraph contrast. The LOWFS/C subsystem work with the primary WFIRST coronagraph architecture called Occulting Mask Coronagraph (OMC) that combines two operating modes: SPC and HLC. These 2 modes share the same LOWFS/C hardware. ZWFS sensor is the sensor (eye) of this LOWFS/C system and will be discussed in detail in this paper.

The paper is structured as follows. Section 2 describes the ZWFS concept, design and analysis parameters; Section 3 covers the extensive sensitivity study on various design parameters for a

*xu.wang@jpl.nasa.gov; phone: 818-393-0229; fax: 818-393-4357; http://www.jpl.nasa.gov

nominal WFIRST-AFTA LOWFS configuration that features an AFTA pupil and a π/2 phase dimple at the focal plane; Section 4 presents the analysis results at SPC and HLC operation modes. The paper is ended with a conclusion in Section 5.

2. ZWFS THEORY & MODEL

2.1 ZWFS theory

The Zernike wavefront sensor is based on the Zernike phase-contrast concept, which was initially proposed by Frits Zernike in the 1930s to enhance the specimen contrast for a microscope by converting specimen's transparent optical phase variations into the intensity variations [1].

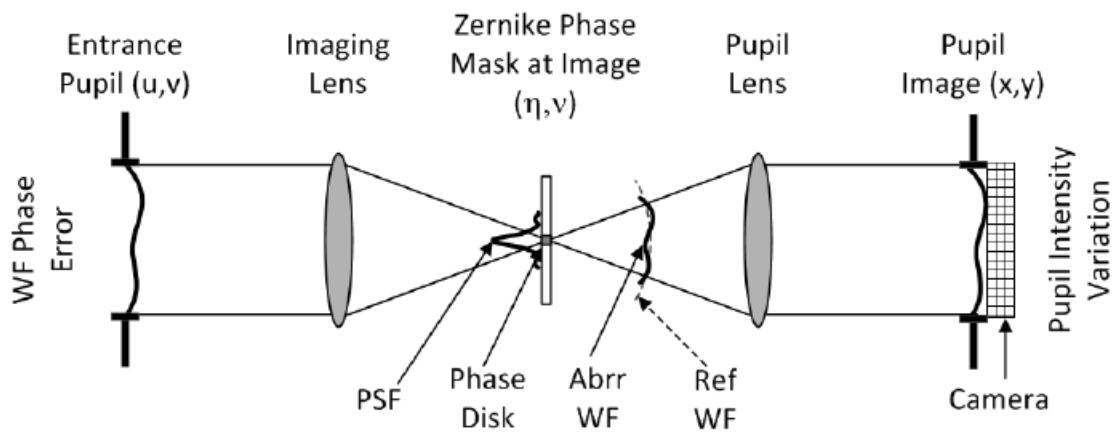

Figure 1 Illustration of Zernike wavefront sensor concept. Lenses are used to represent the optics between entrance pupil, imaging plane, and re-imaged pupil plane.

Figure 1 illustrates the concept of the Zernike wavefront sensor in the context of an astronomical instrument. The WFE is represented by the wavefront phase variation at the entrance pupil plane, such as the primary mirror of a telescope. An imaging system (depicted as an imaging lens in the figure) focuses the starlight to form a point source image referred to as the point spread function (PSF) whose intensity distribution contains the imaging system optical properties such as the pupil geometry and WFEs. In this transmissive configuration a transparent phase disk is placed at the focal plane where the star image is formed, introducing a phase change for the central part of the star image, a region typically ~λ/D in diameter in the PSF space. The light that passes through this small phase disk acts as a reference wavefront (Ref WF in the figure). It interferes with the light passing outside the phase disk which contains the information on wavefront aberrations (Abbr WF in the figure). When the interfered light is reimaged to another pupil, it produces an intensity pattern that is related to the input wavefront aberration (phase error). This intensity pattern can then be detected by a detector such as a CCD camera. The exact intensity encoding of the WFE depends on the phase difference and size of the phase disk, and a quasi-linearity is achieved when the phase disk produces a phase difference of about π/2 radian between the inner and outer parts of the PSF light.

The analytical treatment of the Zernike phase contrast wavefront sensing can be found in many optical textbooks [2,3]. In this paper we follow the treatment used by Wallace [4], where it shows that, with a π/2 phase shift at the Phase Disk in Figure 1, the electrical field and intensity at the output pupil plane can be represented as

$$E = A(e^{i\pi/2} + \varepsilon(u,v) + i\phi(u,v)) = A(i + \varepsilon(u,v) + i\phi(u,v)) \quad (1)$$

$$I = A^2(1 + \varepsilon(u,v)^2 - 2\phi(u,v) + \phi(u,v)^2) \approx A^2(1 + \varepsilon(u,v)^2 - 2\phi(u,v)) \quad (2)$$

Where, A is the mean electric field amplitude, $\varepsilon(u,v)$ is the point-by-point variation in the electric field amplitude, and $\phi(u,v)$ is the pupil-dependent phase.

Eq. 2 can be analytically solved to compute the WFE ϕ from the pupil image intensity I. However, it was also shown in Wallace's paper that the wavefront sensor suffered non-uniform gains across the different Zernike modes and mode cross-talks. In the WFIRST coronagraph the role of LOWFS/C is to maintain the wavefront, so we construct a differential image-based linear algorithm to compute the relative WFE directly from the pupil image intensity. First, the LOWFS/C camera takes the reference image denoted as I_{ref},

$$I_{ref} = A^2(1 + \varepsilon_0^{\ 2} - 2\phi_0) \quad (3)$$

where amplitude variation ε_0 and wavefront phase variation ϕ_0 have been set in the process of creating the coronagraph dark hole. The subsequent wavefront drift $\Delta\phi$ causes the pupil image at LOWFS/C camera to be the "aberrated image" I_{abbr},

$$I_{abbr} = A^2(1 + \varepsilon_0^{\ 2} - 2(\phi_0 + \Delta\phi)) \quad (4)$$

Then the wavefront drift $\Delta\phi$ is proportional to the image difference of the aberrated image and the reference image ΔI by,

$$\Delta\phi = \frac{(I_{abbr} - I_{ref})}{2A^2} = \frac{\Delta I}{2A^2} \quad (5)$$

The WFIRST coronagraph LOWFS/C uses linearized relationship of differential images and WFE to directly detect WFE. To do that we first build a WFE to differential image response matrix $\boldsymbol{K}$. We use the Zernike coefficients to represent the low order WF by a vector $\boldsymbol{Z}$, where $\boldsymbol{Z}=[Z2, Z3, \ldots, Zk]$ with k is typically less than 11 and $\boldsymbol{Z1}$(piston) is not used. We also reorder (vectorize) the two-dimensional differential image ΔI into a vector $\Delta\boldsymbol{L}$. With $\Delta\boldsymbol{L}=\boldsymbol{K} * \boldsymbol{Z}$, $\boldsymbol{K}$ can be first generated with the modeled or experimental measured differential images with the known input amount (α) of each Zernike mode applied to the system, then we can use the pseudo inverse of $\boldsymbol{K}$ to build a reconstruction matrix to detect WFE in the form of Zernike coefficients from the vectorized differential image $\Delta\boldsymbol{L}$:

$$Z = \alpha^{-1}(K^T K)^{-1} K^T \bullet \Delta L \quad (6)$$

It is important to note that in this linear algorithm the ZWFS sensing linearity range is limited to WFE in the neighborhood of the response matrix "training point" α. WFE with amplitude significantly different from α will result in sensing error due to the nonlinearity. Therefore $\boldsymbol{K}$ needs to be built with the training point α near where the WFE would be and α can be different for each Zernike mode. As the analysis results presented in Section 3.1 have shown that the ZWFS has a linearity range, and a Zernike mode response matrix $\boldsymbol{K}$ trained at $\alpha=0.03$ nm the ZWFS maintains linearity better than 1% over 10 nm. This is sufficient to cover a typical WFIRST-AFTA WFE drift.

2.2 Modeling approach, parameter set, and configuration

To analyze the performance of WFIRST LOWFS ZWFS, an end-to-end diffraction model has been developed, utilizing a semi-analytical method (SAM) [5]. SAM provides a fast and memory

efficient alternative to Fourier Transform between pupil and image planes in Lyot-style coronagraphs. For the FFT method, to represent small features of the optical system, both the pupil and the image planes must be finely sampled (with large array size), the Fourier transform of these large array sizes is computationally slow and memory intensive. SAM removes the need of array padding and dramatically lowers the computation requirements. By limiting the region of interest to a square array of side length N_A in the pupil plane and N_B in the image plane, a 2D Fourier transform of the function f(x,y) can be computed by a matrix product:

$$F(u,v) = m/(N_A N_B) * e^{-2i\pi uxT} * f(x,y) * e^{-2i\pi yvT} \quad (7)$$

where m is N_B divided by the scale factor λ/D. The SAM and FFT method yield numerically identical results, but SAM provides a ~35x speed improvement.

Figure 2 shows the ZWFS modeling process (using HLC configuration as an example). The interference of ZWFS turns the wavefront phase error at entrance pupil into the intensity variation at ZWFS's camera. The intensity map that mimics the phase error map becomes obvious in the differentiated image when the DC components from the complex diffraction of the pupil geometry, DMs setting, and phase mask are removed. To model the ZWFS performance, a set of baseline modeling parameters that are consistent with the current coronagraph design have been used to better represent the real system. For photometry, a G type star is used for rejected starlight and the star magnitude varies from Mv=0 to Mv=8. The total effective system transmission is 0.24 which takes into account all of the WFIRST coronagraph optical element throughputs. The ZWFS pupil sampling is 16x16 pixels, which was chosen to optimize the sensor signal-to-noise ratio (SNR) and minimize WFE modes cross-talk (more details seen in Section 3). The detector model is based on the E2V CCD39 chip with 4 e^- read out noise, 1 e^- dark noise at 1 kHz frame rate, and about 80% to 87% quantum efficiency (QE) covering 128 nm spectral band centered at 561 nm (more details seen in Section 3)

Our ZWFS model has three configurations: (1) the simple phase disk configuration where the ZWFS focal plane mask is just a π/2 phase disk of ~1.22 λ/D diameter while the PSF is generated from the WFIRST-AFTA pupil. This is used as a baseline for comparison with ZWFS for HLC and SPC; (2) the HLC configuration where the Focal Plane Mask (FPM) is the HLC occulter and both DMs have special patterns that is an integral part of the HLC design for WFIRST-AFTA coronagraph [6]. Because of the HLC DM patterns the PSF formed on the occulter is no longer an ideal PSF from pupil diffraction as in configuration (1); (3) the SPC configuration where an optimized shaped pupil mask creates a unique PSF with areas of high starlight cancelation. The FPM is a bow-tie shaped occulter with a π/2 phase disk of size ~1.22 λ/D in the center. The results reported in this paper are from the SPC characterization pupil mask design [7]. We also studied another SPC configuration with the SPC discovery pupil mask and the circular FPM. Due to the length of this paper, we do not report the results from SPC discovery mask here since they are similar to SPC bowtie FPM configuration.

3. SENSOR PERFORMANCE & SENSITIVITY

3.1 Sensor performance

ZWFS sensing linearity and cross-talk were evaluated with noise free case. Sensing linearity is to checks, for a certain injected Zernike mode, how much of that aberration can be sensed (i.e., the ratio of sensed Zernike to injected Zernike as a function of input magnitude).

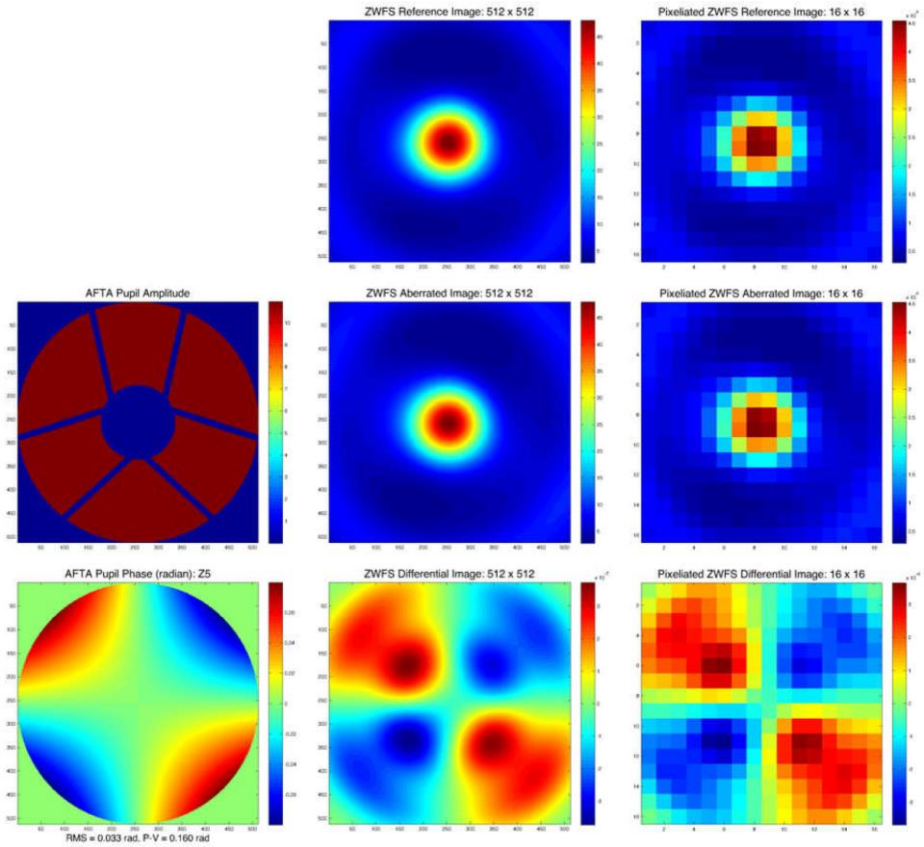

Figure 2 Example images of ZWFS modeling process using the HLC configuration. The images on the left column are the amplitude and phase error at WFIRST-AFTA entrance pupil. Here the phase error is the 45 degree astigmatism mode (Z5). The images in middle column are, from top to bottom, the high resolution ZWFS reference (no phase error) image, the aberrated image, and the differential image. The images on the right column are, from top to bottom, the corresponding pixelated (16x16 pixels) reference, aberrated, and differential images. The differential images mimic the phase error input and the pixelated differential image (lower right) is the signal ΔL used for ZWFS sensing per Eq. 6.

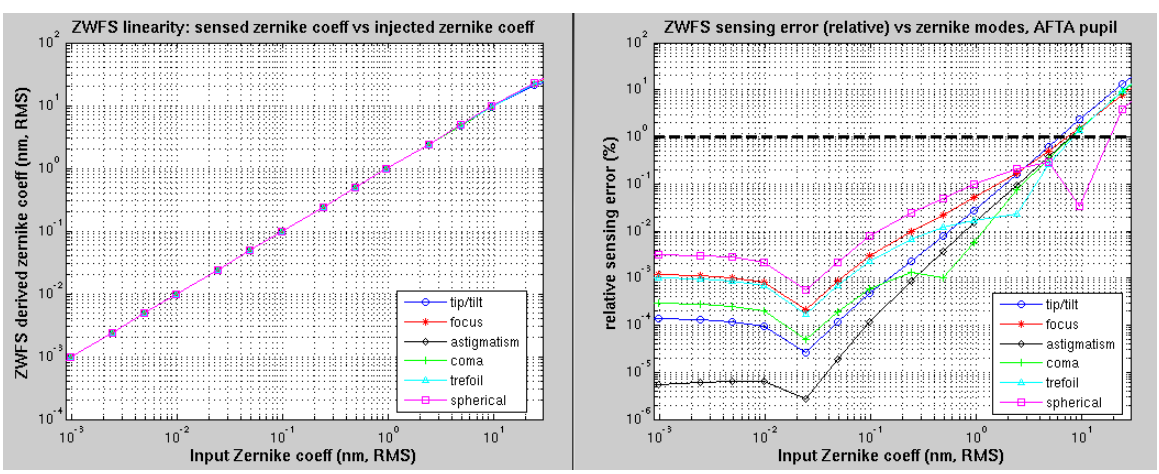

Figure 3 ZWFS sensor linearity for a simple phase disk ZWFS. The plots on the left show the given and the sensed aberration modes with the input WFE expanding from 1 pm to 30 nm. The plots on the right show the percentage sensing error over the WFE range. For this analysis the ZWFS ***training*** matrix is generated with α~ *0.03* nm, where the sensing error minimums occur on the curves on shown on the right.

The sensing error is defined as the difference from the ratio of 1, and is used to evaluate the size of the working range of ZWFS with a predefined sensing error limit. Figure 3 shows the linearity assessment results from the simple phase disk configuration (ZWFS configuration #1). This shows that ZWFS sensing range can be as large as 10nm RMS WFE with a 1% sensing error limit. Breaking down the sensing error further into different Zernike modes shows that the largest sensing errors are for focus aberration and spherical aberration while the smallest sensing errors are for tip/tilt over the linear range.

Sensing cross-talk evaluates for a given Zernike aberration mode how much of the other Zernike modes are erroneously sensed. The cross-talk error is defined as the ratio the largest sensed but un-injected Zernike coefficient to the injected Zernike coefficient. Figure 4 shows the sensing cross-talk from the simple phase disk configuration is less than 0.8% for most of the Zernike modes when the input aberration is at 1 nm RMS. Due to the sensing linearity discussed in the previous section, sensing at larger derivation from the training point will result in larger sensing cross-talk. In other words, the sensing cross-talk is consistent with the sensing linearity.

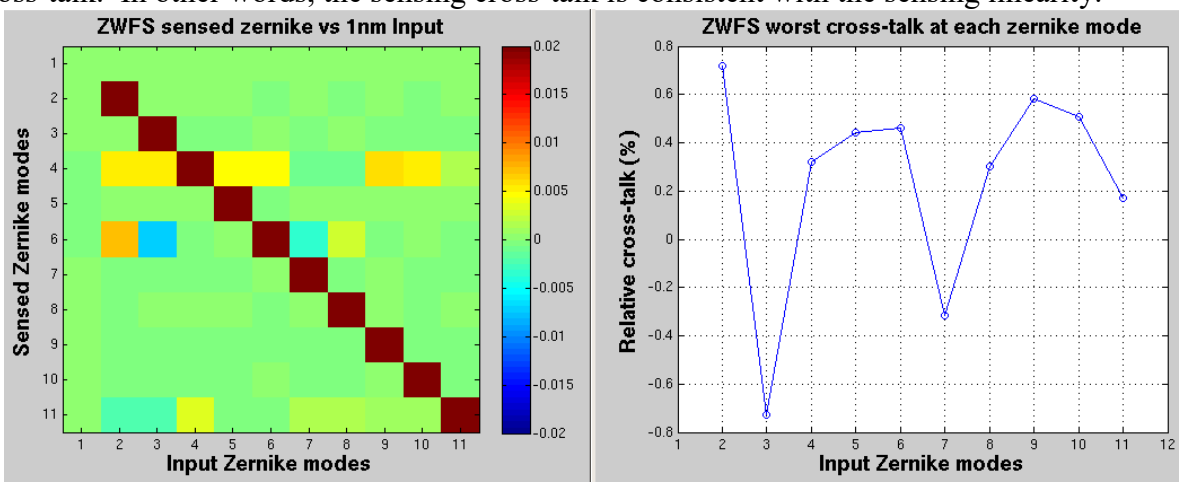

Figure 4 ZWFS sensing crosstalk for a simple phase disk ZWFS. The plot on the left shows cross-talk of Zernike mode sensed vs. Zernike modes input. Each column represents the ZWFS response to a single Zernike input mode of 1 nm RMS. For example column 4 is for a 1 nm focus mode (Z4) input. The plot shows that besides Z4 the ZWFS also senses a small amount of spherical (Z11), which is from the sensor cross-talk of Z4 to Z11. The plot on the right shows the relative cross-talk, i.e., the ratio (percentage) of the worst cross-talk error relative to the input mode.

Another important ZWFS performance metrics is the noise equivalent sensing error. It measures how the sensor performs when the photon and detector noise are present. The ZWFS sensor noise performance analysis is done in the following steps:

1) The ZWFS model generates the ZWFS image with no aberrations
2) Photon and detector noise are added to this image in 100 random realizations
3) For each realization, generate ZWFS differential image and reconstruct the corresponding Zernike coefficients. Since the image was generated when there is no WFE present, the sensed WFE is the noise equivalent sensing errors.
4) Take the average of the 100 random realizations of sensing error to obtain the mean RMS of tilts (Z2, Z3) and OPD (Z4 to Z11) sensing errors to find the noise equivalent sensing error. The noise equivalent tilt is converted to noise equivalent LoS angle.

Figure 5 shows the noise equivalent LoS angle and noise equivalent sensing error for the simple phase dimple model. Notice that the ZWFS noise sensing error is dominated by the photon noise with sensing errors and star magnitudes following a power law curve. Only for fainter stars of Mv > 7, does the noise performance curve begin to deviate from this power law, as the detector noise starts to dominate. It is important to emphasize that this noise performance curve is evaluated at camera readout rate of 1 kHz. For slowly drifting low order WFE, the sensor performance can be improved through image averaging, which is equivalent to increasing the stellar brightness. For example, if we average 1000 camera images (equivalent read out rate of one frame per second), the 0.5 nm sensing error from an Mv = 5 star will be reduced to 16 pm.

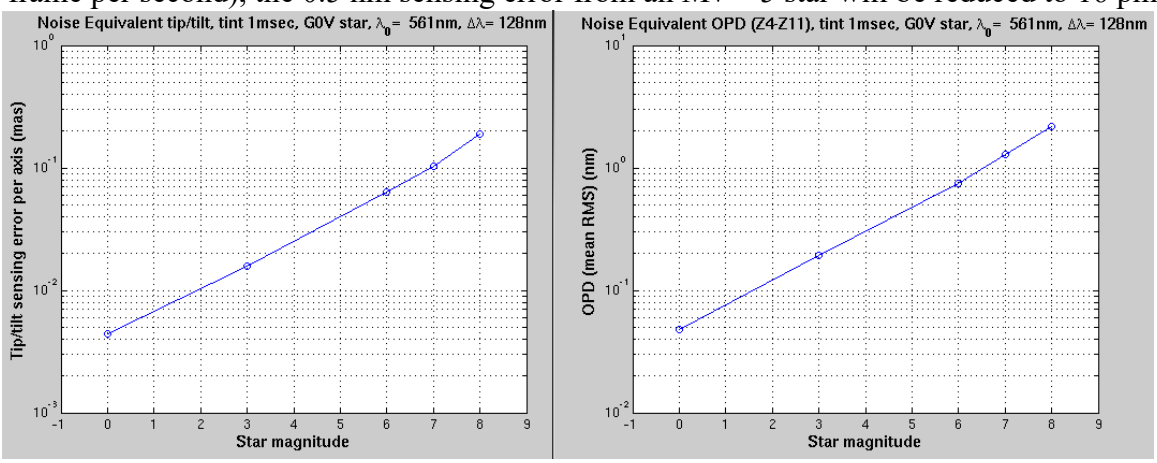

Figure 5 ZWFS noise performance for a simple Zernike phase disk configurations with the ZWFS camera running at 1 kHz frame rate. The plot on the left is the noise equivalent angle and plot on the right is that of noise equivalent low order WF sensing error.

3.2 Sensor performance sensitivity studies

3.2.1 Phase dimple diameter

Figure 6 shows the ZWFS performance with the phase dimple at different radial sizes. The optimal size with the best noise performance is at 1.22 λ/D diameter, ~half of the Airy disk size.

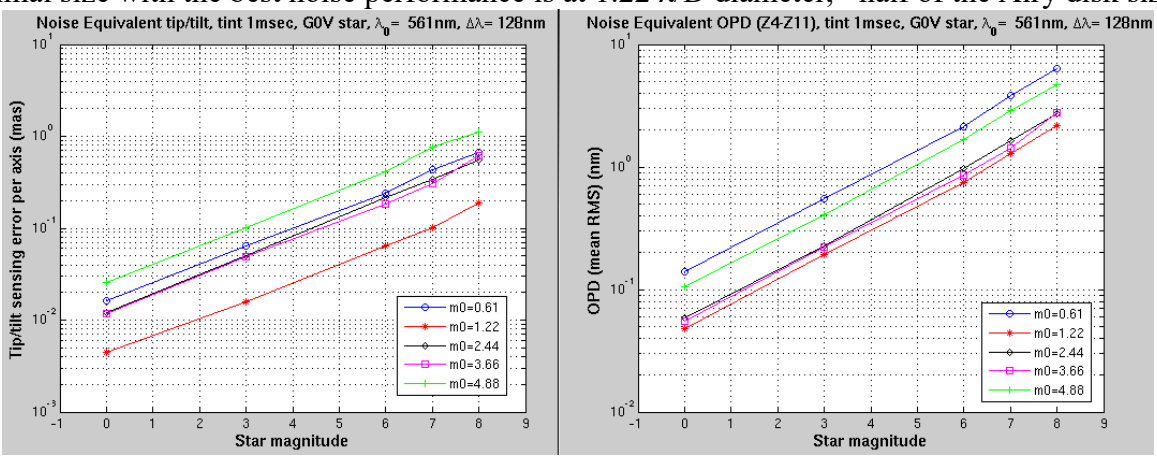

Figure 6 ZWFS noise performance on phase dimple size. The plot on the left shows the effect on noise equivalent angle and the plot on the right is that of low order WFE sensing error.

3.2.2 Source chromatic effect

ZWFS uses a dielectric phase disk at the center focal plane mask to create a phase difference of π/2. The sensor is inherently chromatic. For the light with wavelength different from the center

wavelength the phase delay is no longer exactly π/2 and will degrade the sensing performance. Figure 7 shows this chromatic effect, where a training matrix is first generated for a 41nm spectral band source centering at 550nm. Then two spectral bands with the same bandwidth, but different center wavelengths, are applied to check the sensing performance. As illustrated, the sensor error increases with the derivation from the design/training wavelength. The optimal bandwidth balances the competing needs for more photons (larger bandwidth) against the sensor errors (smaller bandwidths). Further study has shown that, for WFIRST-AFTA ZWFS, the optimal spectral bandwidth is about 128 nm. Sensing performance degrades when the spectral bandwidth is either too narrow (lower photon flux) or too broad (chromatic errors).

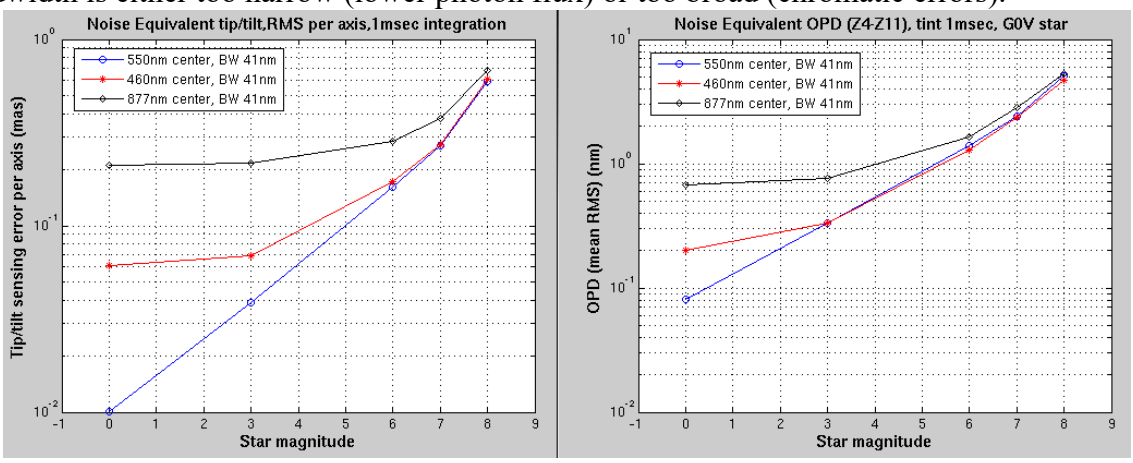

Figure 7 ZWFS chromatic effect. The plot on the left shows the effect on noise equivalent angle and the plot on the right is that of low order WFE sensing error.

3.2.3 Detector quantum efficiency

Detector quantum efficiency (QE) variation, either during manufacturing due to poor quality control or during measurement due to the environment variation, is inevitable in the practical world. Fixed pattern variation can be calibrated out; it is the non-fixed pattern noise on QE that affects our performance analysis. Figure 8 shows, for star brighter than Mv=3 magnitude, QE variation affects the ZWFS performance; but for those dimer stars, we don't see much difference on ZWFS performance because there isn't enough photons to be pulled out of the noise.

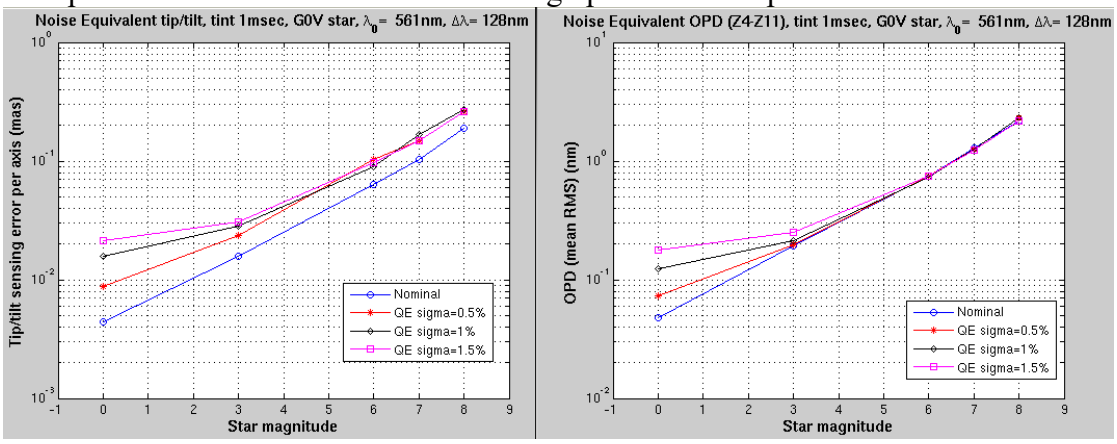

Figure 8 ZWFs noise performance on detector QE variation. The plot on the left shows the effect on noise equivalent angle and the plot on the right is that of low order WFE sensing error.

3.2.4 Image registration

During the ZWFS measurement, two intensity images, reference and measured, will be taken at different times. If the LOWFS/C imaging optics are not stable, causing the two images to shift relative to each other, the mis-registration between the reference and measurement images will cause ZWFS sensing error. We have studied the ZWFS sensitivity to the image mis-registration by creating sub-pixel shift between the two images in the sensor noise performance modeling. Figure 9 shows that, for stars brighter than Mv=3 magnitude, this image mis-registration does affect the ZWFS performance. Fortunately the ZWFS uses pupil image so the image position is not affected by WFE or line-of-sight tilt. Furthermore the ZWFS has a very coarse sampling, 16 pixels across the entire telescope pupil, so this level of registration stability is not that strict.

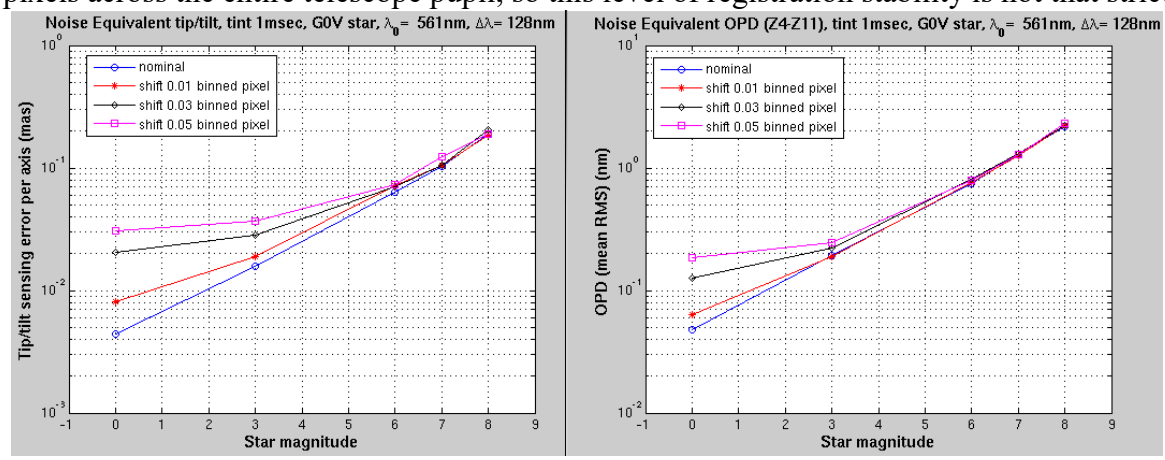

Figure 9 ZWFS noise performance on image mis-registration. The plot on the left shows the effect on noise equivalent angle and the plot on the right is that of low order WFE sensing error.

3.2.5 Detector read noise

The impact of ZWFS camera read out noise is shown in Fig 10. The ZWFS noise performance is evaluated with cameras that has no noise, 4e-, and 30e- read out noise. As expected, as the camera read out noise increases, the ZWFS performance degrades. E2V CCD-39 detector with about 4e- readout noise is currently the baseline ZWFS detector.

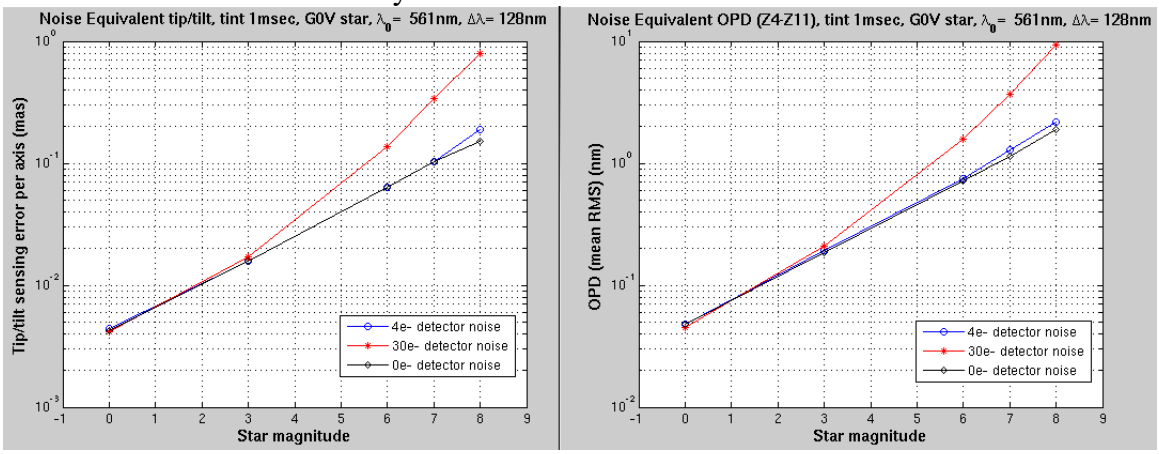

Figure 10 ZWFS noise performance on detector read out noise. The plot on the left shows the effect on noise equivalent angle and the plot on the right is that on low order WFE sensing error.

3.2.6 ZWFS sensor size

This section discusses the effect of sensor size (8x8 to 64x64) on ZWFS performance. Figure 11

shows that sensing size is a tradeoff between sensing resolution and photon flux. When observing bright stars, there are many photons and the noise performance is independent of sensor array size. However, for dim stars detector noise dominates and, binning more pixels (smaller sensor size) does help the noise performance.

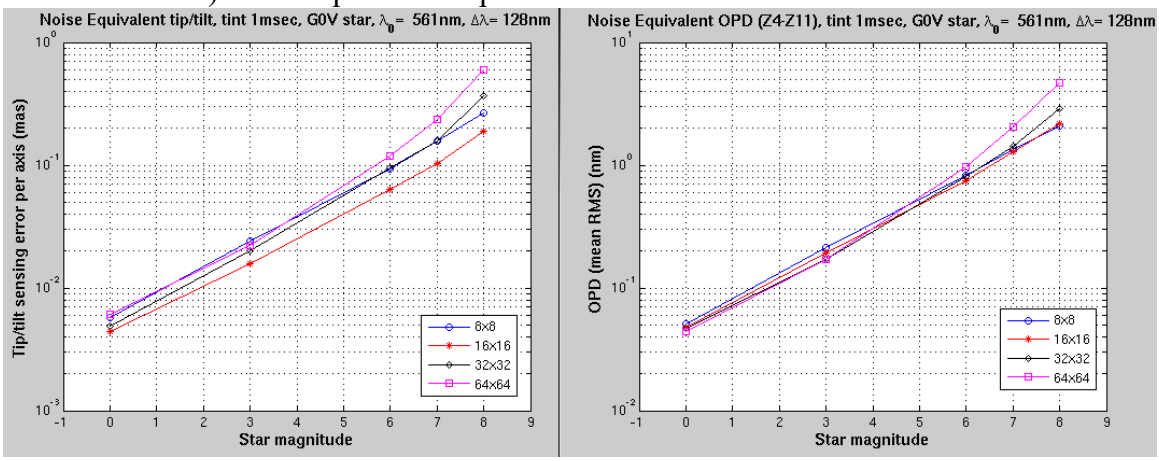

Figure 11 ZWFs noise performance on sensor size. The plot on the left shows the effect on noise equivalent angle and the plot on the right is that on low order WFE sensing error.

3.2.7 ZWFS sensing modes

This section discusses the effect of the number of sensing modes (up to Z11 or Z15) on ZWFS performance. Figure 12 shows sensing more Zernike modes (up to Z15 vs up to Z11) increases the sensing error on OPD (since there will be more Zernike summed up), but does not significantly change the tip/tilt sensing error. Actually, a fairer comparison is to, for the case of sensing up to Z15, only use the result up to Z11, and compare it to the case of sensing only up to Z11. This new comparison shows that their difference is negligible, hinting that our ZWFS sensing model can be applied to higher order wavefront errors as well, if necessary.

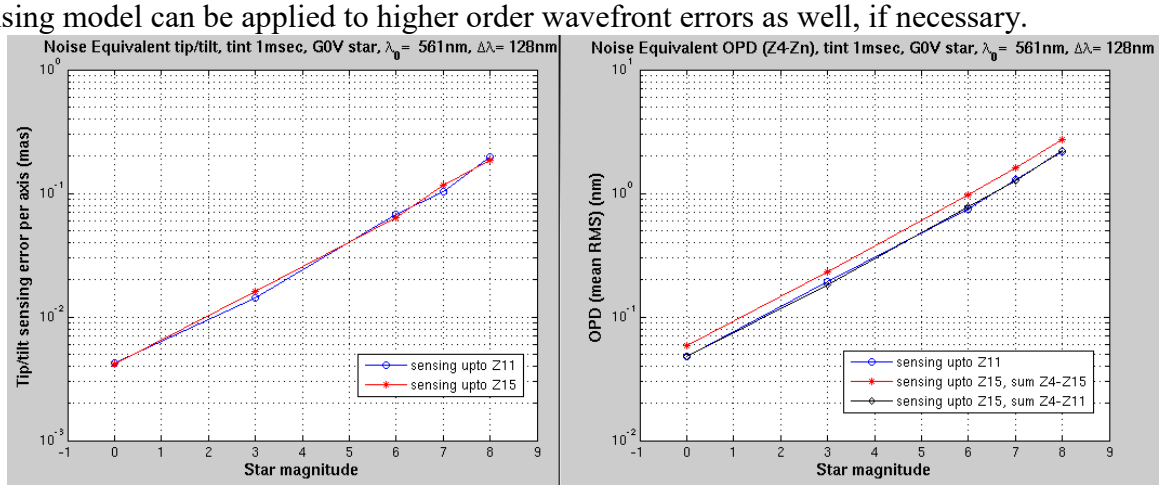

Figure 12 ZWFs noise performance on sensing modes. The plot on the left shows the effect on noise equivalent angle and the plot on the right is that on low order WFE sensing error.

4. SENSOR PERFORMANCE FOR SPC & HLC

Once the analysis parameters are optimized from those various sensitivity studies, the ZWFS model was applied extensively to study/design LOWFS for SPC & HLC configuration. Due to the length of this paper, those analysis results will be reported briefly below.

4.1 SPC configuration

Figure 13 listed two generations of SPC configurations (pupils & focal plane masks). For coronagraph, generation 2 has a smaller inner working angle (it can detect planets that are closer to the star). For LOWFS however, generation 1 has ~1.5x flux of generations 2. This hints that ZWFS performance of generation 1 actually will be better than that of generation 2, which is confirmed in the noise performance chart in Figure 14.

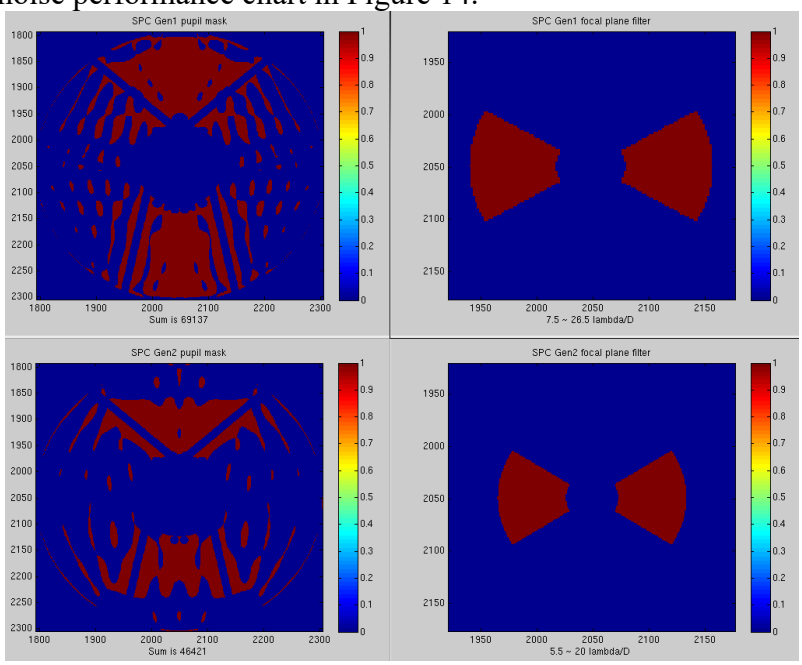

Figure 13 Two generations of SPC pupil and its corresponding focal plane masks.

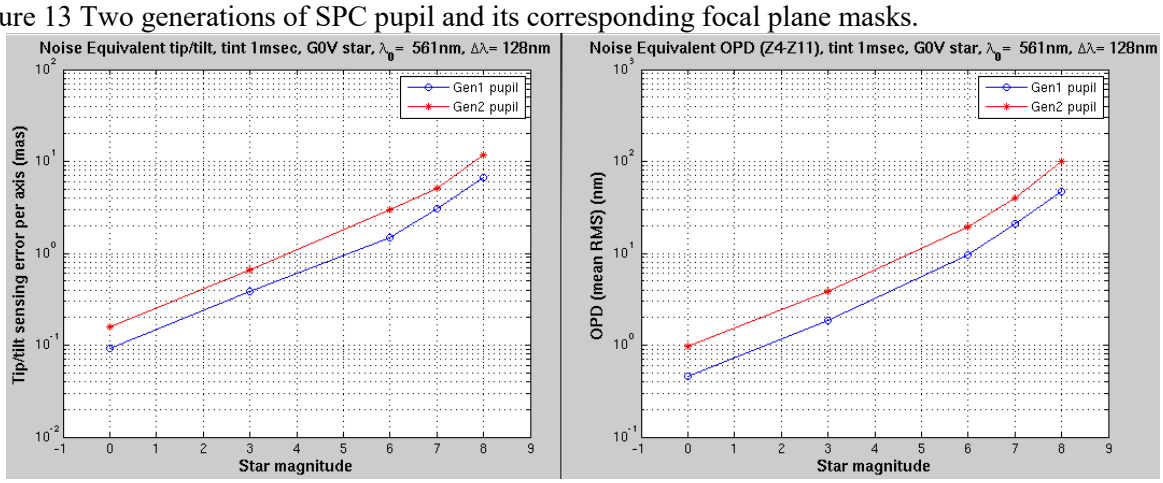

Figure 14 ZWFS noise performance at two SPC configurations. The plot on the left shows the effect on noise equivalent angle and the plot on the right is that of low order WFE sensing error.

4.2 HLC configuration

The HLC phase plate at the focal plane combines the coronagraph phase profile and the ZWFS phase dimple, and creates a common mode on WFE sensing for both coronagraph path and

LOWFS path. Figure 15 shows HLC mask phase profile where the center flat portion is the ZWFS phase dimple and annual rings with different phase modulation are coming from the coronagraph path.

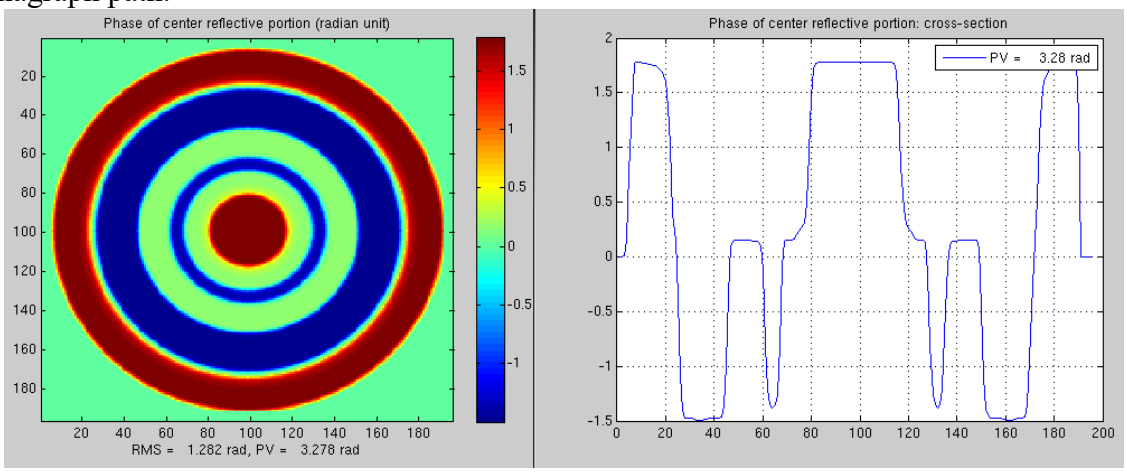

Figure 15 HLC phase profile + LOWFS phase dimple in the center

At HLC configuration, DM settting and coronagrph phase profile are mainly optimized from coronagraph path for science observation. To evaluate their impact on ZWFS noise performance, we analyzed three cases: 1)no DM setting, no coronagraph phase profile, focal plane mask is a reflective disk with outer diameter of 6 λ/D and the 1.22λ/D center portion modulated with a flat π/2 phase; 2)no DM setting, combine coronagraph phase profile with ZWFS phase dimple at the focal plane mask; 3)apply DM setting and coronagraph phase, this is the true HLC configuration. Figure 16 shows the simulated intensities at the output plane with no aberration and the corresponding ZWFS signals (differental images). Due to the filter effect of 6λ/D diameter mask, the intensity pattern at the output plane is different from that of AFTA pupil (higher order components, such as spider pattern, are filtered out). Due to diffraction, the coronagrph phase profile changes intensity pattern further and cuts the total flux by ~65%. The DM setting only slight changes intensity pattern, but cuts the total flux by another ~50%.

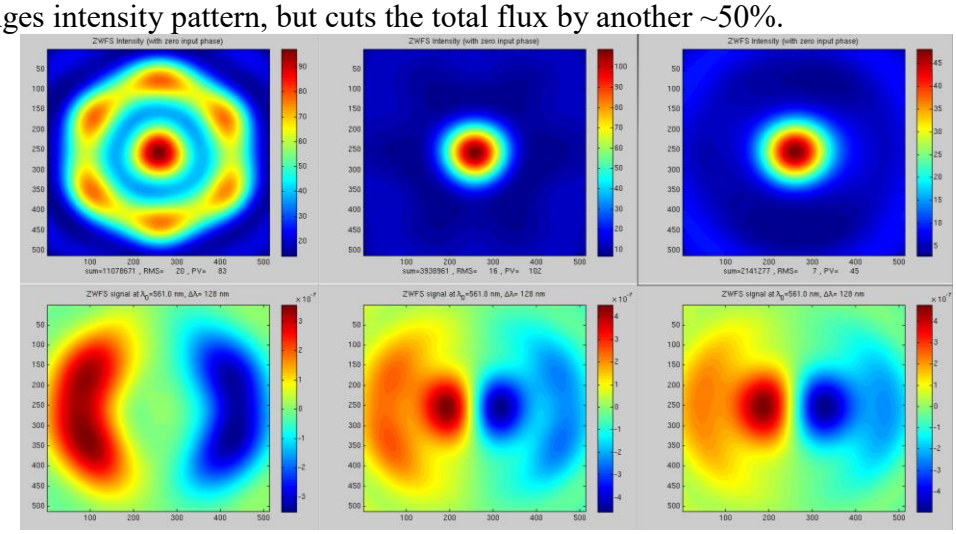

Figure 16 ZWFS intensity patterns and corresponding ZWFS signals at different scenarios. Left column: no coronagraph phase profile and no DM setting; center column: with coronagraph phase profile but no DM setting; right column: with coronagraph phase profile and DM setting.

The ZWFS performance for these above three cases are listed in Figure 17. The comparison shows that coronagraph phase profile degrades performance more than the DM setting does. This is consistent with the flux loss observation.

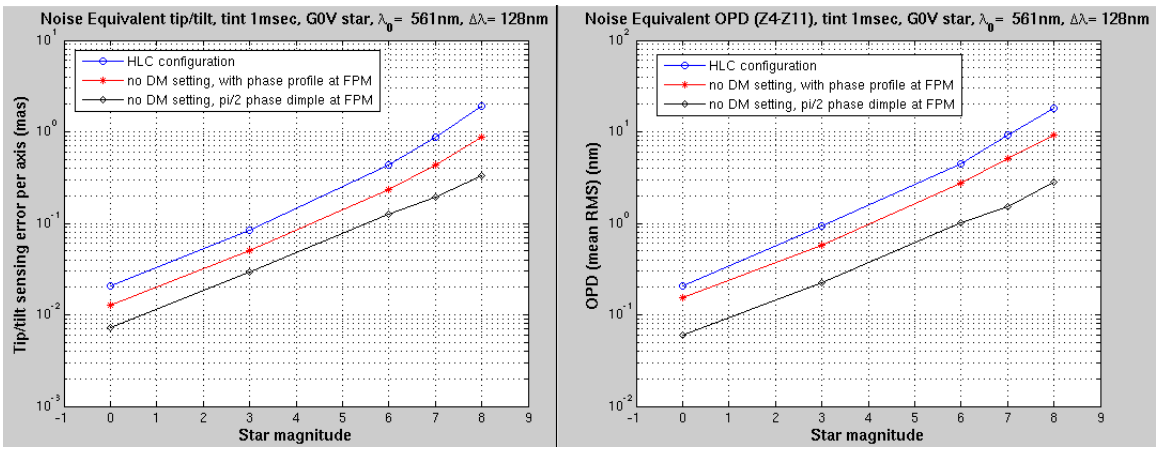

Figure 17 ZWFS noise performance for HLC configuration for three scenarios. Sensitivity on the coronagraph phase profile and the DM setting is reflected in the figure. The plot on the left shows the effect on noise equivalent angle and the plot on the right is that of low order WFE sensing error.

4.3 Performance comparison between simple phase disk, SPC, and HLC configuration

Figure 18 summarizes the ZWFS noise performance for three system configurations. Note that the current configuration setup, such as DM setting and FPM profile, is mainly optimized based on performance of the coronagraph path. LOWFS path simply uses the rejected light for wavefront sensing and control to keep the system stable during the science observation. Nevertheless, this performance summary chart is still useful in the system design trades. For example, for a star magnitude of 5, which is typical in our planned observation, observed in a HLC configuration with 1ms integration time, the ZWFS sensing error on tip/tilt and OPD (Z4toZ11) is less than 0.3mas and less than 3nm, respectively. Finally, the noise performance is not always a pure replication of the flux comparison: HLC has less flux than SPC does. But, HLC noise performance is actually better than SPC noise performance.

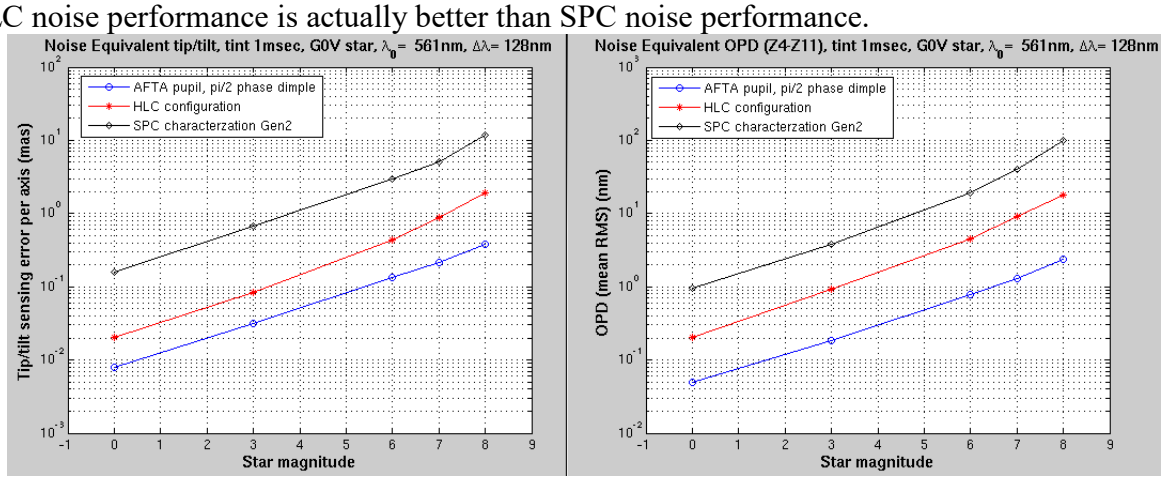

Figure 18 ZWFS noise performance for nominal configuration, HLC, and SPC. The plot on the left shows the effect on noise equivalent angle and the plot on the right is that of low order WFE sensing error.

5. CONCLUSION

The WFIRST coronagraph requires a low order wavefront sensing and control subsystem to maintain the coronagraph's contrast stability. The Zernike phase contrast wavefront sensor is selected to sense the low order wavefront drift and line-of-sight jitter using the starlight rejected by the coronagraph's focal plane mask. A suite of ZWFS models have been developed, thoroughly tested, and used for sensitivity studies on various noises and perturbations. The modeling analysis suggests that ZWFS sensor is capable of detecting sub milliarcsecond tilt, as needed for WFIRST coronagraph to meet its science requirements. A LOWFS/C testbed is being built to simulate WFIRST-AFTA telescope LoS jitter and wavefront drift. The LOWFS/C subsystem will be tested separately before integrating it with the coronagraph.

ACKNOWLEDGEMENT

This research was carried out at the Jet Propulsion Laboratory, California Institute of Technology, under contract with the National Aeronautics and Space Administration (NASA).

REFERENCES

1. K. Zernike, *MNRAS*, **94**, 377 (1934)
2. J. W. Goodman, *Introduction to Fourier Optics*, 2nd Edition, p220-222, McGraw-Hill, (1996)
3. M. Born, E. Wolf, *Principles of optics, Electromagnetic theory of propagation, interference and diffraction of light*, Cambridge, MA, Cambridge University Press, (1999)
4. J. K. Wallace, S. Rao, R. M. Jensen-Clem, G. Serabyn, "*Phase-Shifting Zernike Interferometer Wavefront Sensor*", *Proc. SPIE* **8126**, 81260F-1 (2011)
5. R. Soummer, etal, "*Fast computation of Lyot-style coronagraph propagation*", Optics Express, Vol. 15, No. 24 (2007)
6. J. Trauger, etal, "*Hybrid Lyot Coronagraph for WFIRST-AFTA: coronagraph design and performance metrics*", *JATIS*, in press, 2015
7. K. Balasubramanian, etal, "*WFIRST-AFTA coronagraph shaped pupil masks: Design, Fabrication and Characterization*", *JATIS*, in press, 2015